



Synthesis of novel Mo-Ni@Al₂O₃ catalyst for converting fatty acid esters into diesel-range alkanes with enhanced hydrodeoxygenation selectivity

Xincheng Cao ^{a,b,d,e,f}, Shiyu Wu ^{b,d,e,f}, Jiaping Zhao ^{b,d,e,f}, Feng Long ^{b,d,e,f}, Shuya Jia ^c, Xiaolei Zhang ^c, Junming Xu ^{b,d,e,f,*}, Jianchun Jiang ^{a,b,d,e,f,**}

^a College of Chemical Engineering, Academy of Advanced Carbon Conversion Technology, Huaqiao University, 668 Jimei Boulevard, Xiamen, Fujian 361021, China

^b Institute of Chemical Industry of Forest Products, Chinese Academy of Forestry, Nanjing 210042, China

^c Department of Chemical and Process Engineering, University of Strathclyde, UK

^d Key and Open Lab. on Forest Chemical Engineering, SFA, Nanjing 210042, China

^e National Engineering Lab. for Biomass Chemical Utilization, 210042, China

^f Key Lab. of Biomass Energy and Material, Jiangsu 210042, China



ARTICLE INFO

Keywords:

Hydrolysis of aluminum nitride
Mo-Ni@Al₂O₃ catalyst
Selective hydrodeoxygenation
Diesel-range alkanes

ABSTRACT

Al₂O₃-supported Ni-Mo as a low-cost and efficient bimetallic catalyst has been applied in the hydrodeoxygenation of plant oils or fats for production of high-quality hydrocarbon fuels, but it is still challenge to avoid the serious cleavage of C-C bonds caused by isolated single-metal Ni sites. Herein, we report a novel Al₂O₃-supported Mo-Ni catalyst (Mo-Ni@Al₂O₃) with Ni and Mo sites in close proximity to enhance the hydrodeoxygenation (HDO) selectivity of fatty acid esters. Compared with the conventional Mo-Ni/γ-Al₂O₃ catalyst showing high hydrogenolysis activity for C-C bonds, the Mo-Ni@Al₂O₃ catalyst exhibited higher HDO selectivity towards the diesel-range alkanes. Detailed characterizations reveal that during the synthesis of Mo-Ni@Al₂O₃ catalyst, the loaded Ni species were present in two forms after reduction in a H₂ flow, one is the closely contact of Ni and Mo bimetallic sites and the other is NiAl₂O₄, which enhances the synergistic promoting effect between Ni and Mo sites and inhibits the presence of isolated metallic Ni active sites, thereby exhibiting the enhanced remarkably HDO selectivity towards target products.

1. Introduction

In recent years, owing to the depletion of fossil fuels and increasing concern for dramatic climate change, biofuels as an alternative to fossil fuel have received increasing attention. Generally, biofuels are derived from the conversion of lignocellulosic biomass and bio-derived lipids. The conversion of lignocellulose biomass into biofuels has been widely reported, however, its large-scale production is limited by the complex biomass structure, complicated processing technologies, and varied produced compounds [1,2]. In contrast, bio-derived lipids with the fatty acid/esters as the main components can be efficiently converted into liquid biofuels with high yield and involving fewer processing steps because of its structural similarity with commercial diesel [3–5]. Currently, fatty acid methyl ester (FAME) has been produced at large-scale as the first-generation biofuels via the transesterification

reaction of bio-derived lipid with methanol [6]. However, high oxygen content, low energy density and poor oxidation stability make it difficult to completely replace the petroleum-based fuels [7,8].

Diesel-like hydrocarbon, namely the green diesel or the second-generation biodiesel, can successfully overcome the problems of the FAME and can more compatible with engines, since it does not contain any oxygen elements [9]. To remove the oxygen of the lipid molecules and produce the green biodiesel, the decarbonylation (DCO) and hydrodeoxygenation (HDO) reaction pathways have been proposed [10,11], which the oxygen atoms were removed in the form of CO and H₂O, respectively. Compared with the DCO reaction with a reduction in carbon chain length, the HDO reaction is more suitable to produce liquid biodiesel and valuable chemicals, since it can selectively extract the oxygen atoms and keep the C-C bonds intact. To date, the HDO catalysts mainly focus on the Pd [12–15], Pt [16,17], Ir [18,19], Ru [20,21], Co

* Corresponding author at: Institute of Chemical Industry of Forest Products, Chinese Academy of Forestry, Nanjing 210042, China.

** Corresponding author at: College of Chemical Engineering, Academy of Advanced Carbon Conversion Technology, Huaqiao University, 668 Jimei Boulevard, Xiamen, Fujian 361021, China.

E-mail addresses: xujunming@icifp.cn (J. Xu), bio-energy@163.com (J. Jiang).

[22–24] and Ni-based catalysts [25–28]. Among these catalysts, Ni-based catalysts received the most attention in the production of biofuels due to its high availability, low cost and high hydrogenation activity.

Alumina-supported Ni-Mo catalyst system, as a low cost and rich in metal-acid sites required for the HDO reaction, has been studied extensively. During the deoxygenation of oils, an effective synergy between Ni and Mo species is very important to improve the catalyst activity and HDO selectivity toward the target products, while the presence of isolated single-metallic Ni on the catalyst surface usually results in a high hydrogenolysis activity towards C–C bonds at high temperatures. In existing studies, Al₂O₃-supported Mo-Ni bimetallic catalysts are generally prepared based on the co-precipitation or impregnation method [29–31], for example, typical incipient and wet impregnation methods. Due to the small surface area of support and weak interaction between metal and support, the loading Ni and Mo species using the above-mentioned methods usually display poor metal dispersion, which weakens their synergistic promoting effect and results in a low HDO selectivity towards the target products. Therefore, developing a Al₂O₃-supported Mo-Ni bimetallic catalysts with well-dispersed and intimately contacted Ni and Mo is of significance for converting natural oils and other biomass-derived oxygenates into valuable chemicals and liquid biofuels.

Here, a novel method was reported to synthesize Al₂O₃-supported Mo-Ni catalyst (Mo-Ni@Al₂O₃) with large surface area and well-distribution of metal species by virtue of the hydrolysis properties of aluminum nitride (AlN) (AlN + 3 H₂O → Al(OH)₃ + NH₃) [32,33], and then applied in catalyzing the HDO of fatty acid esters into diesel-range alkanes. The characterization results showed that most of added Ni species exposed on the catalyst surface by interacting with Mo species, and only a small part of Ni species formed catalytically inactive NiAl₂O₄ species after calcination at 400 °C. The interactions between Ni²⁺, Mo⁶⁺, and Al³⁺ ions inhibit the presence of large and isolated Ni nanoparticles, and make the Ni and Mo closely adjacent, which enhances the synergy between Ni and Mo sites and exhibits the improved HDO selectivity towards the diesel-range alkanes. In this work, we investigate the strong interaction between the metal ions, the changes in the morphology, and the phase compositions of the AlN support during the hydrolysis. Based on the results of control experiments and catalyst characterization, the relationship between catalyst structure and activity was revealed. In addition, for comparison, the physico-chemical properties and catalytic reaction mechanism of the conventional Mo-Ni/γ-Al₂O₃ catalyst were also illustrated.

2. Experimental section

2.1. Preparation of Mo-Ni@Al₂O₃ catalyst

The Mo-Ni@Al₂O₃ catalysts were synthesized via the hydrolysis of AlN. Prior to hydrolysis, the AlN support (99.9% metal basis, particle size 50 nm, Macklin) was calcined at 600 °C for 4.0 h in air atmosphere. The calcined support was then gradually introduced into an mixed aqueous solution of Ni(NO₃)₂·6 H₂O (Aladdin) and (NH₄)₆Mo₇O₂₄·4 H₂O (Aladdin), and stirred for 24 h at 40 °C to obtain Mo⁶⁺-Ni²⁺@Al(OH)₃. Subsequently, it was dried at 105 °C for 12 h and calcined at 400 °C for 4 h to obtain the Mo-Ni oxide@Al₂O₃. The loading of Ni related to the support was fixed at 10 wt%, while the loading of Mo species was changed from 0 to 20 wt%. Finally, the catalyst precursor was reduced in flowing H₂ at 500 °C for 3.0 h. These catalysts were denoted as X % Mo-Ni@Al₂O₃ catalysts, where the X refers to the mass loading of the Mo. The actual metal loadings were displayed in Table S1. For comparison, commercial γ-Al₂O₃ (99.9% metal basis, particle size < 50 nm, Aladdin) supported Mo-Ni bimetallic catalyst (10%Mo-Ni/γ-Al₂O₃) with the same metal loading as the 10%Mo-Ni@Al₂O₃ catalyst was also synthesized by using the same method described above, except for the different support. It is noted that the '@' and '/' in the 10% Mo-

Ni@Al₂O₃ and 10% Mo-Ni/γ-Al₂O₃ refer to Al₂O₃-encapsulated and -supported NiMo bimetallic nanoparticles, respectively. The AlN (H) was also prepared via the hydrolysis of pure AlN support at 40 °C as a comparison, and the hydrolysis process was the same as that of Mo-Ni@Al₂O₃ catalyst.

2.2. Catalyst characterization

The crystalline structure and phase composition were measured by the power X-ray diffraction (XRD), which was operated at 40 kV with Cu Kα radiation source ($\lambda = 0.15418$ nm). The XRD patterns were obtained by scanning 20 from 10 ° to 80 ° with 0.05 ° step size. XRD diffraction peaks were identified based on PDF-2 2018 databank by MDI Jade 5.0 software. Raman spectroscopy was collected using a Horiba Jobin Yvon HR 800UV and the excitation wavelength was 532 nm. The surface area and pore size distribution were measured by N₂ adsorption-desorption isotherms at 77 K. The distribution of metal species on the catalyst surface were observed by the Transmission electron microscopy (TEM). XPS spectra were performed on a Thermo Escalab 250XI to analyze the chemical state and the possible interaction between metals. The temperature programmed reduction (H₂-TPR) and NH₃ chemisorption (NH₃-TPD) were carried out on a Micromeritics AutoChem II 2920 apparatus to analyze the interaction between metals and the acid site distributions, respectively, and the operating detailed procedures can be found elsewhere [34]. To study the interaction between catalyst and the fatty aldehyde intermediate, the in-situ spectra of the octanal molecular were performed on the Thermo Nicolet-iS50 FT-IR. Prior to test, the catalyst was reduced in situ at 500 °C for 1.0 h. After that, the system was cooled to room temperature, and the octanal vapor was adsorbed on the catalyst surface until saturation. Then, the system temperature was increased from 25 to 150 °C and held at set the temperature point for 10 min under flowing hydrogen.

2.3. Catalyst activity evaluation

The catalytic performance of catalyst was tested in a 50 mL autoclave reactor. Methyl stearate was selected as model compound for the HDO reaction. Typically, 0.1 g reactant, 10 mL n-hexane and 0.03 g catalyst were introduced into the reactor. Before the reaction, first introduce gas three times with H₂ (2.0 MPa), and then 3.0 MPa H₂ was pressurized into the reactor at ambient temperature. Afterwards, the reactor was heated up to 210 ~ 240 °C at a stirring speed of 1000 rpm. The reaction products were analyzed by gas chromatography (GC). The Eicosane was used as internal standard for the quantification of liquid product. The calculated equations of the conversion and selectivity towards products can be found in our previous work [13]. Each experimental result was repeated at least two times with errors less than 5%, and the results showed in this work were the mean value of repeated experiments.

The hydrodeoxygenation/decarbonylation ratio (HDO/DCO) was calculated according to the following Eq. (1):

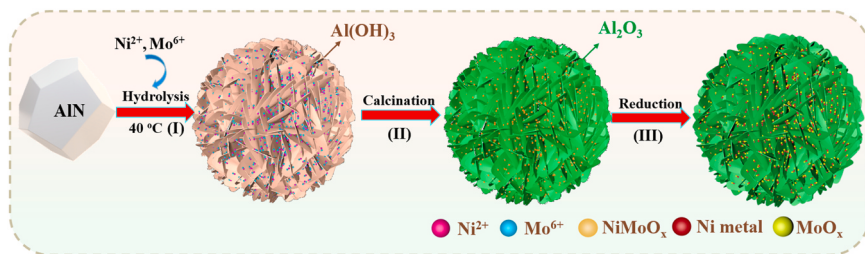
$$\frac{\text{HDO}}{\text{DCO}} \text{ ratio} = \frac{C_{18}}{C_{17}} \times 100\% \quad (1)$$

Where C₁₈ and C₁₇ refer to the molar content of the 1-octodecane and 1-heptadecane, respectively.

3. Results and discussion

3.1. Formation and physical properties of Mo-Ni@Al₂O₃ catalyst

The Mo-Ni@Al₂O₃ catalyst was prepared via the hydrolysis of AlN support, as shown in Scheme 1. First, the metal ions were loaded on the AlN support surface, and then the AlN support begin to hydrolysis to generate Mo-Ni ions encapsulated by aluminum hydroxide. In this process, the surface area gradually increased and the mesopores were



Scheme 1. Schematic diagram of the Mo-Ni@Al₂O₃ catalysts prepared by hydrolysis of AlN support.

created, as evidenced in the N₂ adsorption-desorption characterization (Fig. 1 (J) and Table S2). The increasing surface area and strong interaction between Al³⁺ and Ni²⁺ ions promoted the dispersion of Ni species, while the interaction between Ni²⁺ and Mo⁶⁺ inhibited the formation of catalytic inactive NiAl₂O₄ compound after calcination, as proved in the H₂-TPR and XPS (Fig. 3). Subsequently, the dried sample

was calcined at 400 °C for 4 h to form NiMoO_x@Al₂O₃ precursor. Finally, the precursor was reduced at 500 °C for 3.0 h to form the Mo-Ni@Al₂O₃ catalyst with large surface area and intimately contacted Ni and Mo sites.

TEM results showed that the AlN support without hydrolysis exhibited a bulk structure (Fig. 1(A)), whereas, after the hydrolysis, the

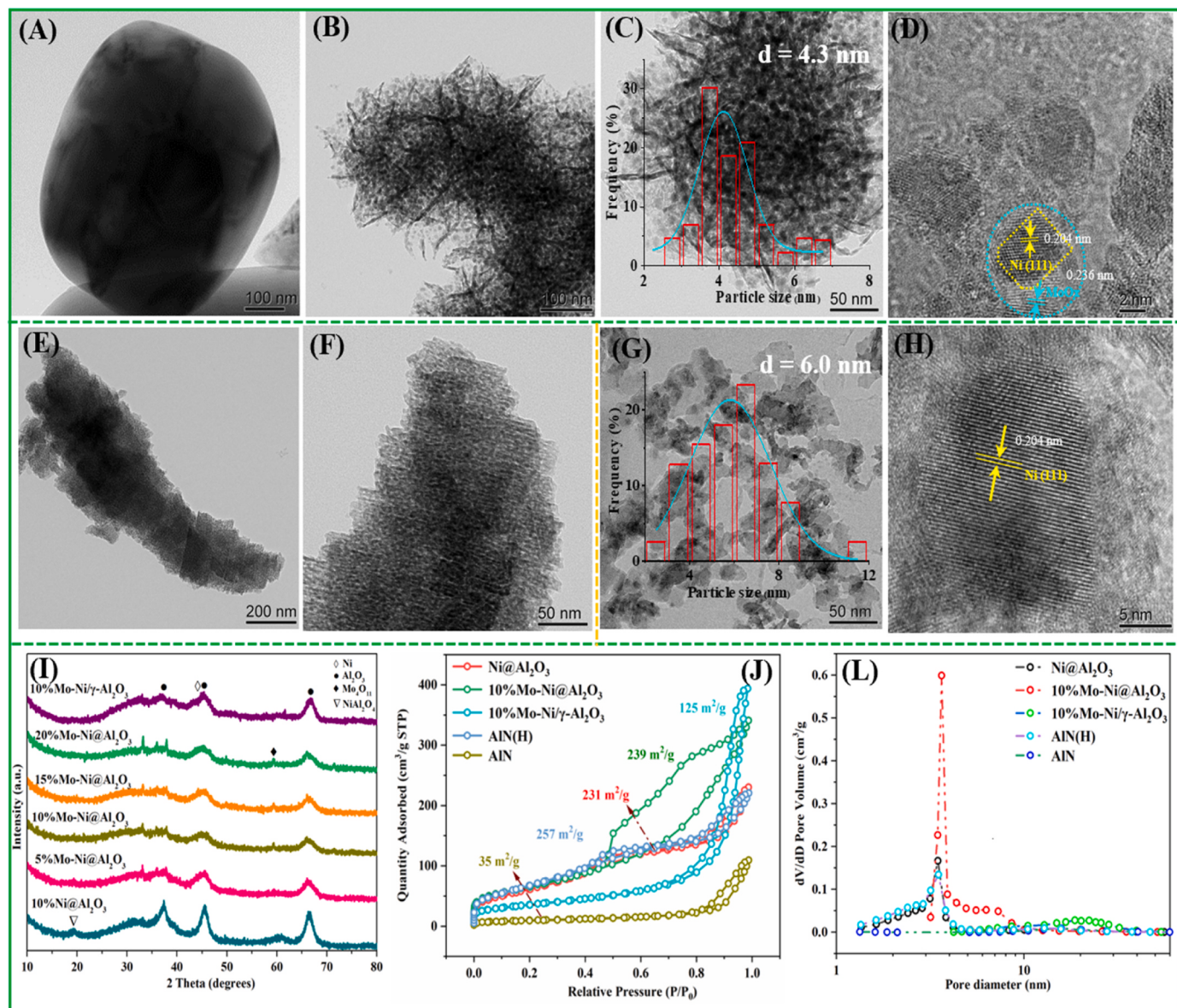


Fig. 1. (A) TEM image of the untreated AlN; (B-C) TEM images of 10%Mo-Ni@Al₂O₃ catalyst; (D) HRTEM image of 10%Mo-Ni@Al₂O₃ catalyst; (E, F) TEM images of Ni@Al₂O₃ catalyst; (G, H) TEM image of 10% Mo-Ni/γ-Al₂O₃ catalyst; (I) XRD patterns; (J) N₂ adsorption-desorption isotherms; (L) pore size distributions curves of the catalysts.

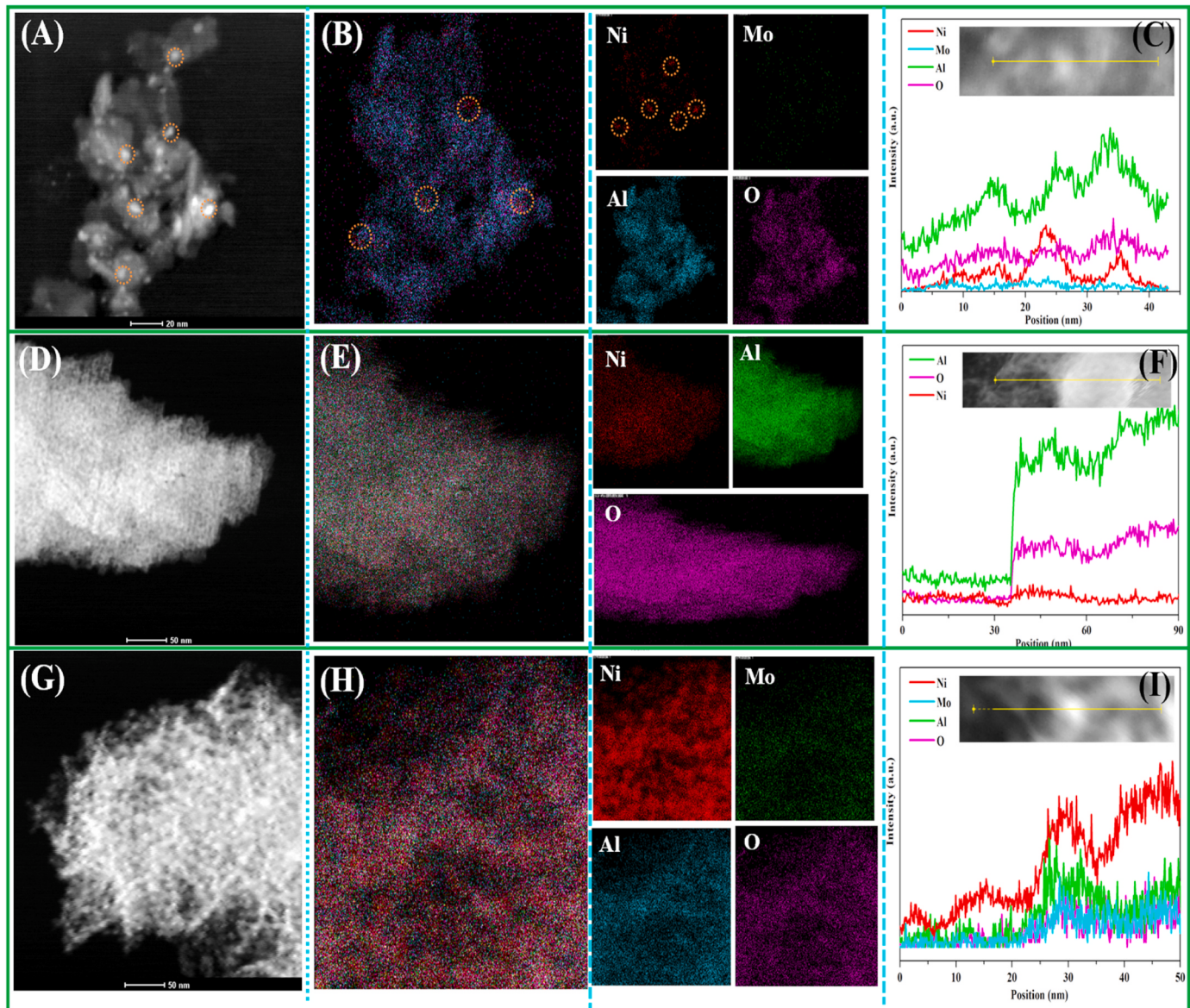


Fig. 2. (A) STEM, (B) EDS elemental mappings, (C) line-scanning analysis of the 10% Mo-Ni/γ-Al₂O₃ catalyst; (D) STEM, (E) EDS elemental mappings, (F) line-scanning analysis of the Ni@Al₂O₃ catalyst; (G) STEM, (H) EDS elemental mappings, (I) line-scanning analysis of the 10% Mo-Ni@Al₂O₃ catalyst.

obtained AlN (H) (Fig. S1 (A, B)), Ni@Al₂O₃ (Fig. 1(E, F)), and Mo-Ni@Al₂O₃ (Fig. 1(B-C)) catalysts presented a lamellar structure with some mesopores. This structural transformation from bulk to lamellar leads to a large surface area of AlN (H), Ni@Al₂O₃, and Mo-Ni@Al₂O₃ catalysts (as listed in Table S2) and promotes the dispersion of metal species on the catalyst surface to some extent. Compared with the Ni@Al₂O₃ catalyst without observing any nanoparticles on the surface (Fig. 1(E–F)), some uniformly dispersed black metal nanoparticles were observed on the Mo-Ni@Al₂O₃ catalyst with the average particle size of 4.3 nm (Fig. 1(B–D)). Basing on the XRD (Fig. 1 (I)) and H₂-TPR characterizations (Fig. 3(A)), this may be due to the fact that in the preparation of the Ni@Al₂O₃ catalyst, the added nickel species participated in the formation of the NiAl₂O₄ by interacting with aluminum ions so that the nickel species were highly dispersed on the catalyst surface. However, this interaction can be weakened by introducing Mo species, since the introduced Mo species can interact with nickel species to form NiMoO₄ compounds, as indicated in the Raman characterization (Fig. 3 (B)). Therefore, much more metallic Ni active sites are exposed on the surface of the Mo-Ni@Al₂O₃ catalyst (Fig. 1(C)) and are closely adjacent with Mo species (Fig. 1(D)). Additionally, the conventional Mo-Ni/

γ-Al₂O₃ catalyst was also characterized for comparison, and showed amorphous structure and much larger metal Ni nanoparticles (the average size was about 6.0 nm) (Fig. 1(G–H)) than that of the Mo-Ni@Al₂O₃ catalyst.

The specific surface area and pore size distribution of the catalyst were analyzed by the N₂-adsorption and desorption (Fig. 1(J and L)), and the detailed parameters are shown in Table S2. The AlN support and the Mo-Ni/γ-Al₂O₃ catalyst showed a small surface area with the 35 m²/g and 125 m²/g, respectively. In contrast, the AlN (H), Ni@Al₂O₃, and Mo-Ni@Al₂O₃ catalysts exhibited a large surface area with the 257 m²/g, 231 m²/g, and 239 m²/g, respectively. Moreover, it is noted that the three catalysts showed type-IV isotherms with type H3 hysteresis loops, which indicates a mesoporous characteristic [35,36]. Their average pore size were 4.7 nm, 5.5 nm, and 8.3 nm, respectively. These results suggest that the Mo-Ni@mesoporous Al₂O₃ catalyst with high metal dispersion and large surface area can be successfully synthesized via the hydrolysis of AlN support.

To identify the composition of the catalysts and observe the metal distribution on the catalyst surface, STEM images and EDS element mappings were performed. As shown in Fig. 2(B, E, H), the Ni and/or Mo

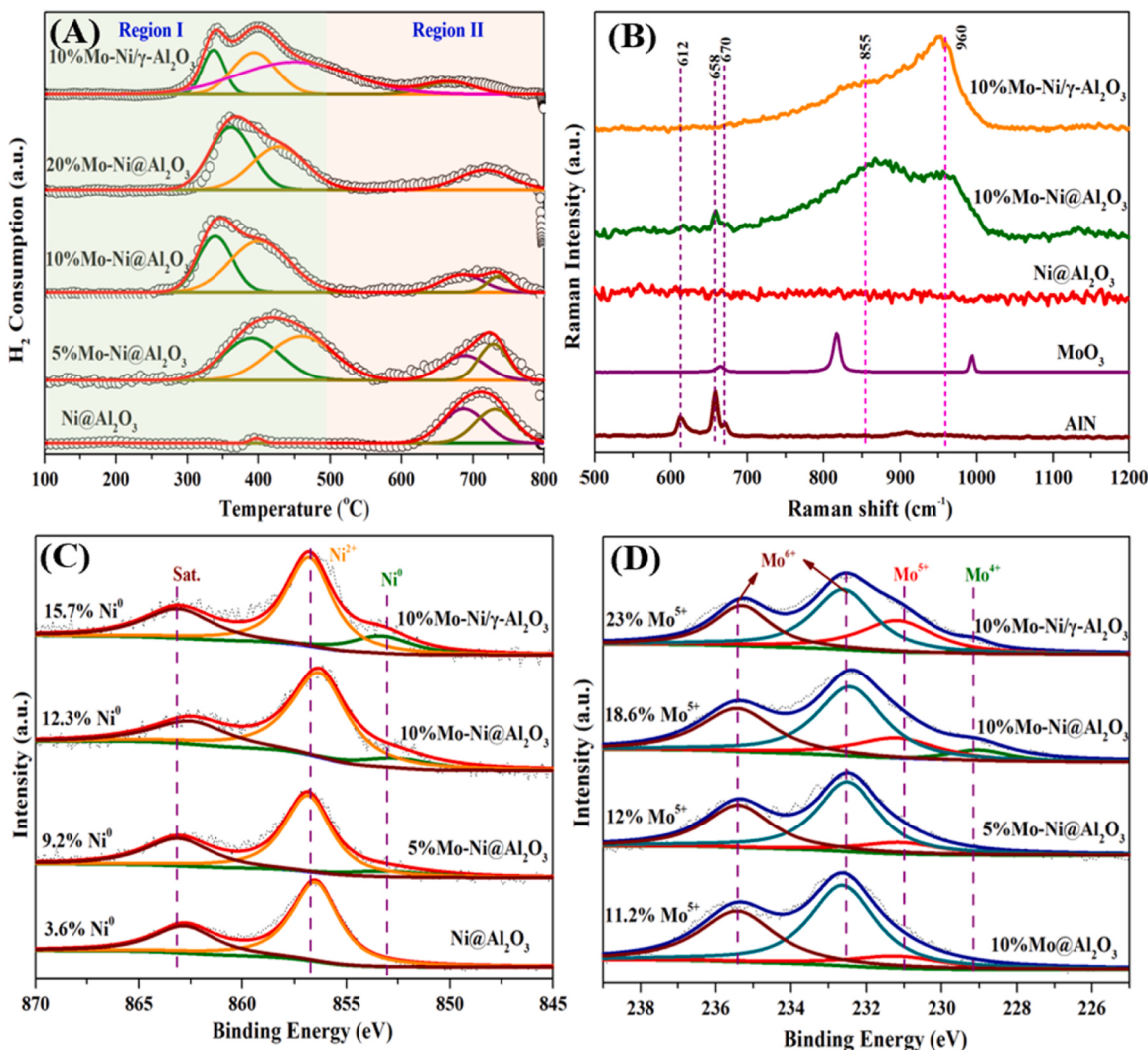


Fig. 3. (A) H₂-TPR profiles, and (B) Raman spectra of calcined catalysts; (C) XPS spectra of the Ni 2p and (D) Mo 3d of the reduced catalysts.

species were successfully dispersed on the surface of the Ni@Al₂O₃, Mo@Al₂O₃, and Mo-Ni/γ-Al₂O₃ catalysts. Compared with the Mo-Ni/γ-Al₂O₃ catalyst with large Ni metal nanoparticles and uneven distribution of metal species (Fig. 2(A–C)), the Ni and Mo species were well-distributed on the surface of the Mo-Ni@Al₂O₃ catalyst (Fig. 2(G–H)). Besides, according to the line-scanning EDS characterization (Fig. 2(I)), it was observed that the EDS profiles of Ni and Mo species exhibited similar trend, which further proved that the two metal species were well-distribution on the surface of Mo-Ni@Al₂O₃ catalyst. For the Ni@Al₂O₃ catalyst, the main difference from the Mo-Ni@Al₂O₃ and Mo-Ni/γ-Al₂O₃ catalysts is that there are no obvious metal nanoparticles observed on the catalyst surface (Fig. 2(D–E)), and the peak intensity of the Ni element is very low (Fig. 2(F)) under the identical nickel loading. One possible explanation is that the added Ni species are incorporated in the alumina lattice. Based on the XRD (Fig. 1(I)) and H₂-TPR (Fig. 3(A)) characterizations, this may be attributed to the strong interaction between Ni²⁺ and Al³⁺ to form many small NiAl₂O₄ nanoparticles during the synthesis of Ni@Al₂O₃ catalyst. Introducing Mo species can inhibit greatly the interaction and make much more metallic Ni nanoparticles expose on the catalyst surface, as illustrated in the Section 3.2.

3.2. Effect of Mo species on the catalysts

The effect of Mo species on the Ni@Al₂O₃ catalyst was studied by H₂-TPR, Raman and XPS characterizations. H₂-TPR results (Fig. 3(A))

showed that the Ni@Al₂O₃ catalyst displayed a very small hydrogen consumption peak with centered at about 400 °C (the reduction of NiO) [37,38] and a broad peak with centered at about 700 °C (the reduction of NiAl₂O₄) [33,39]. The major consumption peak appeared in the high temperature of 700 °C indicates that there is a very small amount of NiO on the surface of Ni@Al₂O₃ catalyst and most of Ni species are presented in the form of NiAl₂O₄. In contrast, the Mo-Ni@Al₂O₃ bimetallic catalysts with different Mo contents displayed a very different reduction behavior from the Ni@Al₂O₃ catalyst, revealing that there is an interaction between Ni and Mo species. For the Mo-Ni@Al₂O₃ catalysts, the major hydrogen consumption peak appeared at low temperature of 500 °C. With an increased in the Mo content, the peak intensity gradually enhanced, while the peak intensity located in the high temperature of 700 °C gradually decreased. Of course, a contribution of Mo species reduction (Mo⁶⁺ to Mo⁴⁺ (reduction temperature: 400–620 °C) and Mo⁴⁺ to Mo⁰ (reduction temperature: 620–800 °C)) to the H₂-TPR curve should not be excluded. But combining with the changes of peak areas of Mo-Ni@Al₂O₃ catalysts at high temperature region (700 °C) that gradually decreases with the addition of Mo species, it can be inferred that the introduction of Mo species inhibits the formation of NiAl₂O₄. This is agreement with the result reported by Kordouli et.al [29]. Additionally, the H₂-TPR spectra of the Mo-Ni/γ-Al₂O₃ catalyst was also investigated for comparison. As shown in Fig. 3(A), the major H₂ consumption peak appeared in the low temperature of 300–500 °C, indicating that the NiO and/or NiMo₄ were dominant on the catalyst surface.

To further explore the interaction between Ni and Mo species, Raman spectra were performed and the results are shown in Fig. 3(B). The Raman spectra of AlN and MoO₃ were also included in the figure. For the Ni@Al₂O₃ catalyst, there was no any peaks observed, indicating that the AlN support has been completely hydrolyzed and the introduced Ni species were highly dispersed on the catalyst surface, in accordance with the results observed in the TEM images (Fig. 1(F)). Compared with the Ni@Al₂O₃ catalyst, the Mo-Ni@Al₂O₃ and Mo-Ni/γ-Al₂O₃ bimetallic catalysts showed two new broad peaks at about 855 cm⁻¹ and 960 cm⁻¹, which corresponds to the characteristic peak of Mo monomeric species [29] and NiMoO₄ [40,41], respectively. Additionally, the spectra of the Mo-Ni@Al₂O₃ catalysts did not show any bands of the crystalline MoO₃ (665, 818, and 995 cm⁻¹) [42], indicating that the dispersion of Mo species is high. Based on the above characterization results, it can be inferred that Mo species weaken the strong interaction between Ni and Al ions mainly through forming highly dispersed NiMoO₄ and monomeric Mo species, which inhibits the formation of NiAl₂O₄ compounds.

Fig. 3(C) and (D) show the XPS spectra of the Ni 2p3/2 and Mo 3d with corresponding deconvoluted peaks for each sample, respectively. It can be seen from Fig. 3(C), after the Ni@Al₂O₃ catalyst was reduced at 500 °C, the binding energy at 853.7 eV attributed to the metallic Ni (Ni⁰) was rarely determined and the content of Ni metal (Ni⁰) only accounted for the percentage of 3.6%. The main peak at 856.0 eV ascribed to the Ni²⁺ species was predominated in the Ni@Al₂O₃. This result indicates that most of added Ni species participated in the formation of NiAl₂O₄ in the Ni@Al₂O₃ catalyst, which is in line with the H₂-TPR results. When the Mo species were introduced, the amount of Ni⁰ species exhibited a gradually increasing trend, which increased from 9.2% of the 5% Mo-Ni@Al₂O₃ catalyst to 12.3% for the 10% Mo-Ni@Al₂O₃ catalyst. This increasing trend can be attributed to the interaction between Ni and Mo, which inhibits the formation of NiAl₂O₄. In comparison, the Ni⁰ content in the 10% Mo-Ni/γ-Al₂O₃ catalyst was also calculated and showed a high Ni⁰ content (15.7%). Since the γ-Al₂O₃ is a commercial stable support and there is little interaction between Ni²⁺ and Al³⁺, therefore, the NiAl₂O₄ was rarely formed on the surface of the Mo-Ni/γ-Al₂O₃, as indicated in the H₂-TPR (Fig. 3(A)). However, as shown in Fig. 2(A), large Ni metal nanoparticles and uneven-distribution of the loading metal species were usually generated on the surface of γ-Al₂O₃ support due to the weak interaction between metal and support, which is undesirable for the selective HDO reaction of fatty acid esters.

Fig. 3(D) shows the spectra of the Mo 3d of the Mo@Al₂O₃ and Mo-Ni@Al₂O₃ catalysts. Deconvoluted peaks revealed a mixture of different oxidation states (Mo⁴⁺, Mo⁵⁺ and Mo⁶⁺) for each sample [41,43]. Compared with the 10% Mo@Al₂O₃ catalyst, the 10% Mo-Ni@Al₂O₃ and 10% Mo-Ni/γ-Al₂O₃ catalysts showed a high amount of Mo⁵⁺ species, indicating that the metallic Ni promotes the reduction of Mo oxide. With an increased in the Mo content, the amount of Mo⁵⁺ species exhibited an increasing trend from 12% (5% Mo-Ni@Al₂O₃) to 18.6% (10% Mo-Ni@Al₂O₃). Among the tested catalysts, the Mo-Ni/γ-Al₂O₃ catalyst showed the highest Mo⁵⁺ content (23%), which may be related to more metallic Ni sites on its surface.

According to the above characterization results of calcined and reduced catalysts, a simplified schematic structure of the different catalysts is shown in Fig. 4. For the monometallic Ni@Al₂O₃ catalyst, the introduced Ni species were participated in the formation of catalytic inactive NiAl₂O₄ compounds due to the strong interaction between Ni²⁺ and Al³⁺, and only a small amount of metallic Ni nanoparticles was determined on the catalyst surface, as proved in H₂-TPR and XPS characterizations (Fig. 3). By contrast, for the Mo-Ni@Al₂O₃ bimetallic catalyst, due to the interaction between Ni and Mo species, the most of added Ni species formed NiMoO₄ compounds by interacting with Mo species and the remaining small part of Ni species participated in the formation of NiAl₂O₄ compounds after calcination at 400 °C in air, as demonstrated in the H₂-TPR and Raman spectra (Fig. 3 (A) and (B)). Therefore, after reduction at 500 °C under H₂ flow, more metallic Ni

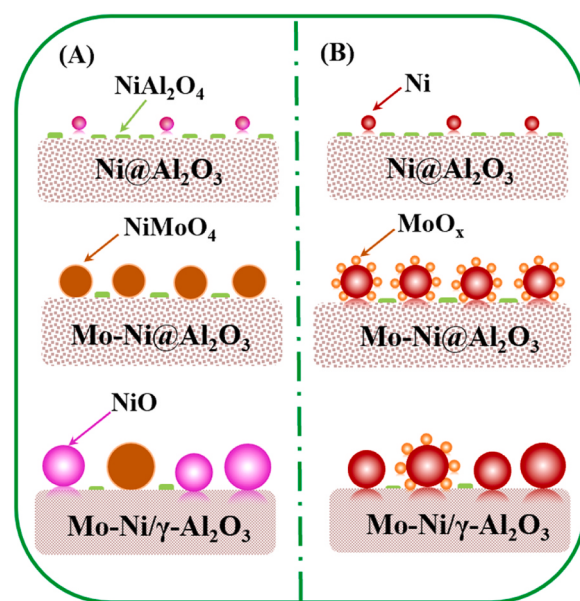


Fig. 4. Schematic structure of the Ni@Al₂O₃, Mo-Ni@Al₂O₃ and Mo-Ni/γ-Al₂O₃ catalysts (A) calcination at 400 °C for 4.0 h in air, (B) reduction at 500 °C for 3.0 h in a H₂ flow.

nanostructures can be detected on the surface of Mo-Ni@Al₂O₃ catalyst than that on the Ni@Al₂O₃ catalyst. As for the conventional Mo-Ni/γ-Al₂O₃ catalyst, STEM and elemental mapping images (Fig. 2(A–C)) showed that some large and isolated metallic Ni nanoparticles were observed on the catalyst surface after reduction, which is probably attributed to the small surface area and the chemical inertness of γ-Al₂O₃ support. The main difference between the Mo-Ni@Al₂O₃ and Mo-Ni/γ-Al₂O₃ was that the interactions between the Ni-Al and Ni-Mo ions in the Mo-Ni@Al₂O₃ catalyst promote the dispersion of Ni species and make Ni and Mo species closely adjacent, as described in Fig. 4, which enhances the synergy between Ni and Mo species and decreases the hydrogenolysis activity of Mo-Ni@Al₂O₃ catalyst towards C–C bonds.

The surface acidity of catalysts was determined by NH₃-TPD, and the results are shown in Fig. 5(A). For the reference AlN support without any treatment, it displayed two weak desorption peaks at about 100 and 300 °C, indicating that the commercial AlN support contains a small amount of acid sites. However, the amount of acid sites increased remarkably after the hydrolysis. In the case of AlN (H), several major ammonia desorption peaks located at about 100 ~ 450 °C can be clearly observed, which corresponds to the weak (T < 300 °C) and medium acid sites (300 °C < T < 450 °C) [29,44]. Among these catalysts, AlN (H) catalyst exhibited the highest amount of total acid sites with 1.82 mmol/g calculated by fitting the peak area. After introducing the Ni and/or Mo species (Ni@Al₂O₃ and Mo-Ni@Al₂O₃ catalysts), the amount of acid sites exhibited a decreasing trend. This is probably because the loading metal species covered the acidic sites of Al₂O₃. The above results indicate that the acid sites of the Ni@Al₂O₃ and Mo-Ni@Al₂O₃ catalysts mainly originate from the aluminum oxide. Additionally, it is noted that the desorption peak shape, position and area of the Ni@Al₂O₃ and 10% Mo-Ni@Al₂O₃ catalysts are similar with those of the 10% Mo-Ni/γ-Al₂O₃ catalyst, suggesting that the catalysts prepared by the hydrolysis of AlN have a similar amount and strength of acid sites as those of the commercial γ-Al₂O₃ supported Mo-Ni catalyst.

In addition to studies on the acidity, the oxygen vacancies have also been determined as an important deoxygenation active site. As shown in Fig. 5(B), the 10% Mo-Ni@Al₂O₃ and 10% Mo-Ni/γ-Al₂O₃ catalysts created more oxygen vacancies than the Ni@Al₂O₃ catalyst under the identical treatment conditions, which indicates that the number of the oxygen vacancy can be enhanced through introducing Mo species. The

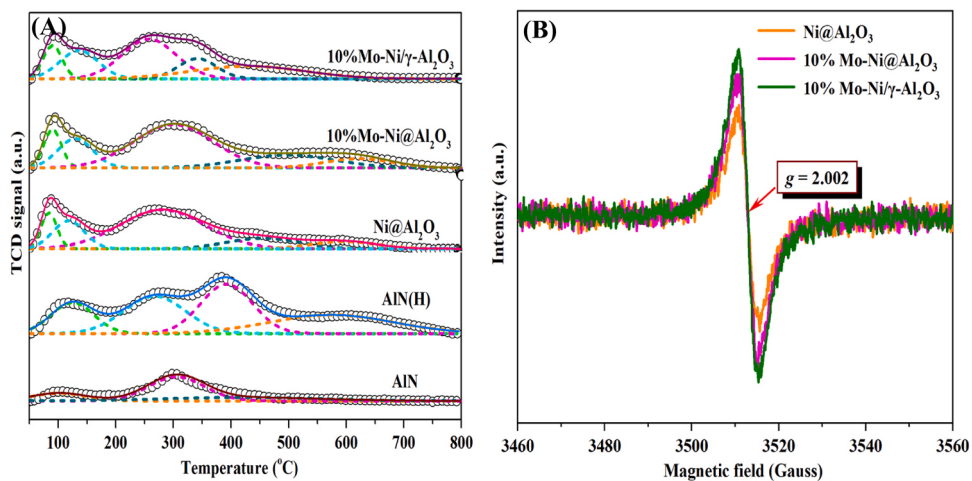


Fig. 5. (A) NH₃-TPD profiles and (B) EPR spectra of the reduced catalysts.

10% Mo-Ni@Al₂O₃ and 10% Mo-Ni/γ-Al₂O₃ catalyst exhibited the similar peak intensity at $g = 2.003$, an indication of the electron trapping at oxygen vacancies [45], indicating that they have similar oxygen vacancy concentrations.

3.3. Catalyst performance evaluation and catalyst stability

The catalyst activity was evaluated in the hydrogenation of methyl stearate and the results are shown in Table 1. After 5.0 h reaction, the main products were n-heptadecane (n-C₁₇), n-octadecane (n-C₁₈) and some intermediate compounds such as the 1-octadecanal (C₁₈-CHO) and 1-octadecanol (C₁₈-OH). The reference AlN support and the Mo@Al₂O₃ catalysts exhibited very low conversion (Table 1, entry 1 and 3, respectively), while the Ni@Al₂O₃ catalyst showed a medium conversion, giving 42.7% conversion and 56% diesel-range alkanes selectivity with C₁₇ alkane being the main product (Table 1, entry 2). This result indicates that the metallic Ni is the catalytically active sites for the conversion of methyl stearate owing to the ability to dissociate hydrogen. Compared with the monometallic Ni@Al₂O₃ catalyst, the Mo-Ni@Al₂O₃ catalyst with different Mo contents presented not only an excellent catalytic performance (>80% conversion) but also a high HDO/DCO ratio (Table 1, entries 4 and 6–8). Superior catalytic

performance was obtained over the 10% Mo-Ni@Al₂O₃ catalyst with > 99% conversion and 96% selectivity to diesel-range alkanes (Table 1, entry 4). Increasing the Mo content to 20 wt%, the catalytic performance was decreased and the intermediate of 1-octadecanol become the main product with 50% selectivity (Table 1, entry 8). According to the XRD characterization (Fig. 1(I)), the decreased catalyst activity over the 20% Mo-Ni@Al₂O₃ can be ascribed to the excessive loading of Mo species, which covered the part of metallic Ni active sites.

Additionally, it was observed that under the identical reaction conditions and metal loadings, the traditional 10%Mo-Ni/γ-Al₂O₃ catalyst also showed excellent catalytic performance with > 99% conversion and 99% selectivity towards diesel-range alkanes (Table 1, entry 5). However, compared to 10% Mo-Ni@Al₂O₃ catalyst with high HDO/DCO ratio (HDO/DCO = 3.2), a low HDO/DCO ratio of 1.2 was obtained over the 10%Mo-Ni/γ-Al₂O₃. These results suggest that the Mo-Ni/γ-Al₂O₃ and Mo-Ni@Al₂O₃ catalysts remove the oxygen atom of the reactant via different reaction pathway, that is, the decarbonylation reaction (DCO) mainly occurred on the Mo-Ni/γ-Al₂O₃ catalyst, while the hydro-deoxygenation reaction (HDO) is dominant on the Mo-Ni@Al₂O₃ catalyst. According to the previous reports, it is known that alumina-supported monometallic Ni is conductive to result in the cleavage of C–C bonds [22], while the synergy between Ni and Mo is beneficial to improve the HDO selectivity [13,43]. Therefore, it is speculated that the high HDO/DCO ratio obtained in the Mo-Ni@Al₂O₃ catalyst can be attributed to the enhanced synergy between the Ni and Mo species. In order to prove the crucial role of the synergy between Ni and Mo species, a physical mixture of Ni@Al₂O₃ and Mo@Al₂O₃ was tested, and showed better catalytic performance and a higher HDO/DCO ratio than that of the Ni@Al₂O₃ catalyst (Table 1, entry 9). However, these results are lower than those of the Mo-Ni@Al₂O₃ catalyst, indicating the crucial role of the intimately contacted Mo and Ni species.

Having identified 10% Mo-Ni@Al₂O₃ catalyst as the best catalyst among the synthesized Mo-Ni@Al₂O₃ catalysts, optimizations of the reaction time at 230 °C were performed to obtain a high yield of target products (Fig. 6(A)). Within 1.0 h, the main products were 1-octadecanol (C₁₈-OH) and 1-octadecanal (C₁₈-CHO) intermediates with the C₁₈-OH being the primary product. As the reactant converted, the selectivity of intermediates decreased gradually, while the n-heptadecane (n-C₁₇) and n-octadecane (n-C₁₈) increased until to the maximum value of 99% during the reaction of 6.0 h. Besides, it is noted that in the different reaction stages, the selectivity of n-C₁₈ alkane is higher than that of the other alkanes, which further proves that the HDO reaction pathway is dominant over the 10% Mo-Ni@Al₂O₃ catalyst. Fig. 6(B) shows the influence of the temperature on the product distribution. At a low temperature of 210 °C, the main product was C₁₈-OH with a selectivity of 40% whereas the alkane selectivity was only 38%. As the temperature

Table 1
Comparison of methyl stearate conversions over different catalysts ^a.

Entry	Catalyst	Conversion/%	Selectivity/%		HDO/DCO
			n-C ₁₇	n-C ₁₈	
1	AlN	< 5.0	—	—	—
2	Ni@Al ₂ O ₃	42.7	48.1	8.3	39.4
3	10% Mo@Al ₂ O ₃	< 5.0	—	—	—
4	10%Mo-Ni@Al ₂ O ₃	> 99	22.8	73.5	0.4
5	10%Mo-Ni/γ-Al ₂ O ₃	> 99	45.3	53.6	—
6	5%Mo-Ni@Al ₂ O ₃	98.0	15.1	31.5	6.9
7	15%Mo-Ni@Al ₂ O ₃	> 99	12.7	50.8	16.6
8	20%Mo-Ni@Al ₂ O ₃	84.2	10.2	35.6	2.8
9	Ni@Al ₂ O ₃ + 10% Mo@Al ₂ O ₃	59.3	17.0	19.5	14.7
					48.7
					1.1

^a Reaction conditions: methyl stearate (0.1 g), catalyst (0.03 g), n-hexane (10 mL), 230 °C, 3.0 MPa H₂, 5.0 h.

^b A = 1-octadecanal, B = 1-octadecanol.

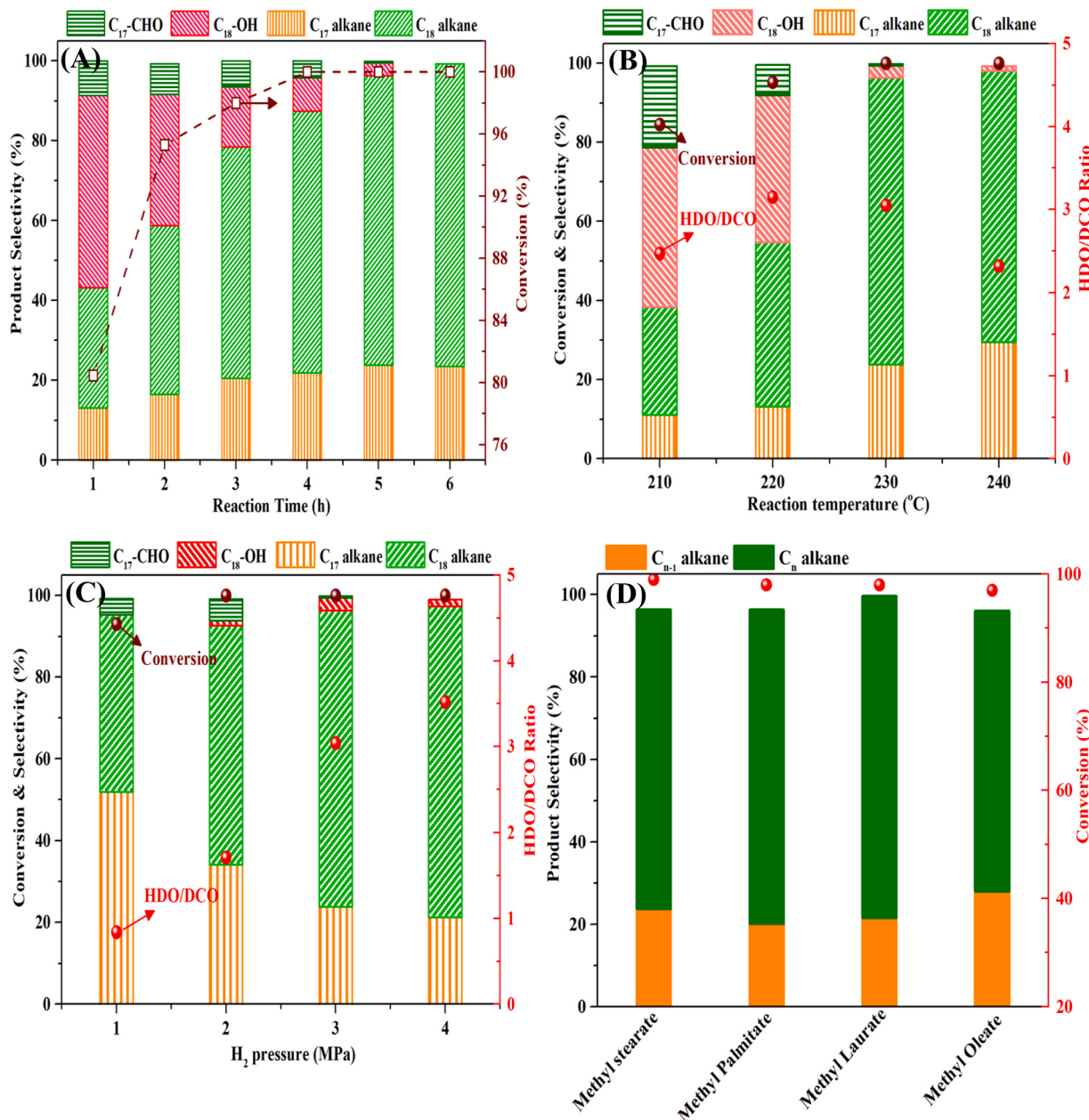


Fig. 6. Reaction parameters optimization over the 10% Mo-Ni@Al₂O₃ catalyst (A) reaction time, (B) temperature, (C) H₂ pressure. (D) HDO of various fatty acid esters over the 10% Mo-Ni@Al₂O₃ catalyst. General reaction conditions: substrate (0.1 g), catalyst (0.03 g), n-hexane (10 mL), 230 °C, 3.0 MPa H₂, 5.0 h.

increased from 210 °C to 230 °C, the selectivity of alkane enhanced significantly to the 96% at 230 °C. Further raising the temperature to 240 °C, the selectivity of alkane reached the maximum value of 99%. Different from the effect of reaction temperature on the reactant conversion, although the hydrogen pressure has less effect on the conversion of reactant, it has a great effect on the HDO/DCO ratio. As shown in Fig. 6(C), at a low H₂ pressure of 1.0 MPa, the HDO/DCO ratio was only 0.8, while the ratio was raised to 3.2 when the H₂ pressure increased to 3.0 MPa. This indicates that high H₂ pressures are beneficial for the HDO selectivity of the reactant, which is consistent with our previous results obtained on the Pd@Al-mSiO₂ catalyst [13]. Based on the principle of the minimum energy consumption, 5.0 h of reaction time, 230 °C of reaction temperature and 3.0 MPa of H₂ pressure were selected to perform the following experiments in this work. Then, various fatty acid esters containing different carbon-chain length were tested over the 10% Mo-Ni@Al₂O₃ catalyst under the selected reaction conditions. As shown in Fig. 6(D), the selected fatty acid esters were completely converted into

the corresponding alkane products with the C_n alkane being the main product, indicating that the 10% Mo-Ni@Al₂O₃ catalyst is an effective catalyst for the HDO reaction of fatty acid esters. To further highlight the excellent catalytic performance of the 10% Mo-Ni@Al₂O₃ for the conversion of fatty acid esters, its catalytic performance was compared with the previously reported catalyst system (Table S3), and showing that the 10% Mo-Ni@Al₂O₃ has superior catalytic performance than them.

Catalyst stability is crucial for heterogeneous catalyst to determine its potential for industrial application, thus the reusability of the 10% Mo-Ni@Al₂O₃ was evaluated. After the reaction, the catalyst and liquid products were separated by centrifugation. The recovered catalyst was directly used to perform the next cycle, and the results are shown in Fig. S2. After the three cycles, the reactant conversion and the selectivity of alkanes were 93% and 87%, respectively. The XPS measurement (Fig. S3) reveals that the decrease of the activity and product selectivity could be attributed to the partial oxidation of metallic Ni and unsaturated Mo species (Mo⁵⁺) during the reaction.

3.4. Analysis of the structure-activity correlation

To explain why the Mo-Ni@Al₂O₃ catalyst shows a good catalytic performance (high catalytic efficiency and high HDO/DCO ratio), a series control experiments with intermediates (C₁₈-CHO and C₁₈-OH) being reactants were performed over the Ni@Al₂O₃, Mo-Ni@Al₂O₃ and Mo-Ni/γ-Al₂O₃ catalysts. Fig. 7(A) shows the conversion of intermediate C₁₈-CHO over the different catalysts. First, we can clearly see that all tested catalysts showed high catalytic performance (>95% conversion) for the hydrogenation of C₁₈-CHO under the selected conditions. Considering that the Ni@Al₂O₃ catalyst exhibited a lower conversion rate (43%) than the Mo-Ni@Al₂O₃ catalysts (>80%) in the conversion of methyl stearate (Table 1, entries 4 and 6–8), it is speculated that the role of Mo species mainly reflects in promoting the conversion of fatty acid esters owing to its strong oxophilicity and inhibition towards the formation of catalytically inactive NiAl₂O₄ compounds, which enhances the adsorption and conversion of fatty acid esters. Besides, it is observed that their product distributions are quite different. Monometallic Ni@Al₂O₃ catalyst gave the C₁₈-OH as the primary product with a selectivity of 72%, while the Mo-Ni@Al₂O₃ catalyst gave the alkanes as main products with n-C₁₈ alkane being the dominant product. This suggests that introducing Mo species is not only beneficial for the conversion of reactant but also for the selective production of n-C₁₈ alkane. In comparison, the catalytic performance of Mo-Ni/γ-Al₂O₃ catalyst was

also tested, and exhibited high catalytic efficiency (100% conversion and 99% total selectivity of alkanes). However, the HDO/DCO ratio of 1.26 indicates that the DCO and HDO reaction pathways occur simultaneously on the Mo-Ni/γ-Al₂O₃ catalyst, as described in Fig. 7 (C).

Fig. 7(B) shows the conversion of intermediate C₁₈-OH over the selected catalysts. After reaction at 3.0 h, the products were alkanes including n-C₁₇ and n-C₁₈ alkanes. Ni@Al₂O₃ and Mo-Ni@Al₂O₃ catalysts gave the n-C₁₇ and n-C₁₈ alkane as the main product, respectively. This result reveals that the dehydrogenation-decarbonylation process of the intermediate C₁₈-OH is dominant over the Ni@Al₂O₃, while the dehydration-hydrogenation process of C₁₈-OH can be enhanced via introducing Mo species, as described in Fig. 7(C), which further confirmed by a series kinetic experiments displayed in Fig. S4. Additionally, it is observed that 10% Mo-Ni/γ-Al₂O₃ showed similar selectivity towards C₁₇ and C₁₈ alkanes with 43% and 56%, respectively. Based on the NH₃-TPD characterization (Fig. 5(A)), it is known that the Ni@Al₂O₃, 10% Mo-Ni/γ-Al₂O₃ and 10% Mo-Ni@Al₂O₃ have similar acid site strength and distribution, therefore, the influence of acidity on the catalytic performance can be excluded. Compared with the Ni@Al₂O₃ catalyst, the superior catalytic activity and high HDO selectivity of 10% Mo-Ni@Al₂O₃ can be attributed to the introduction of Mo species. On one aspect, it inhibits the formation of catalytically inactive NiAl₂O₄, which provides more hydrogenation active sites (Ni⁰) for the hydrogenation reaction. On the other hand, its strong oxophilicity

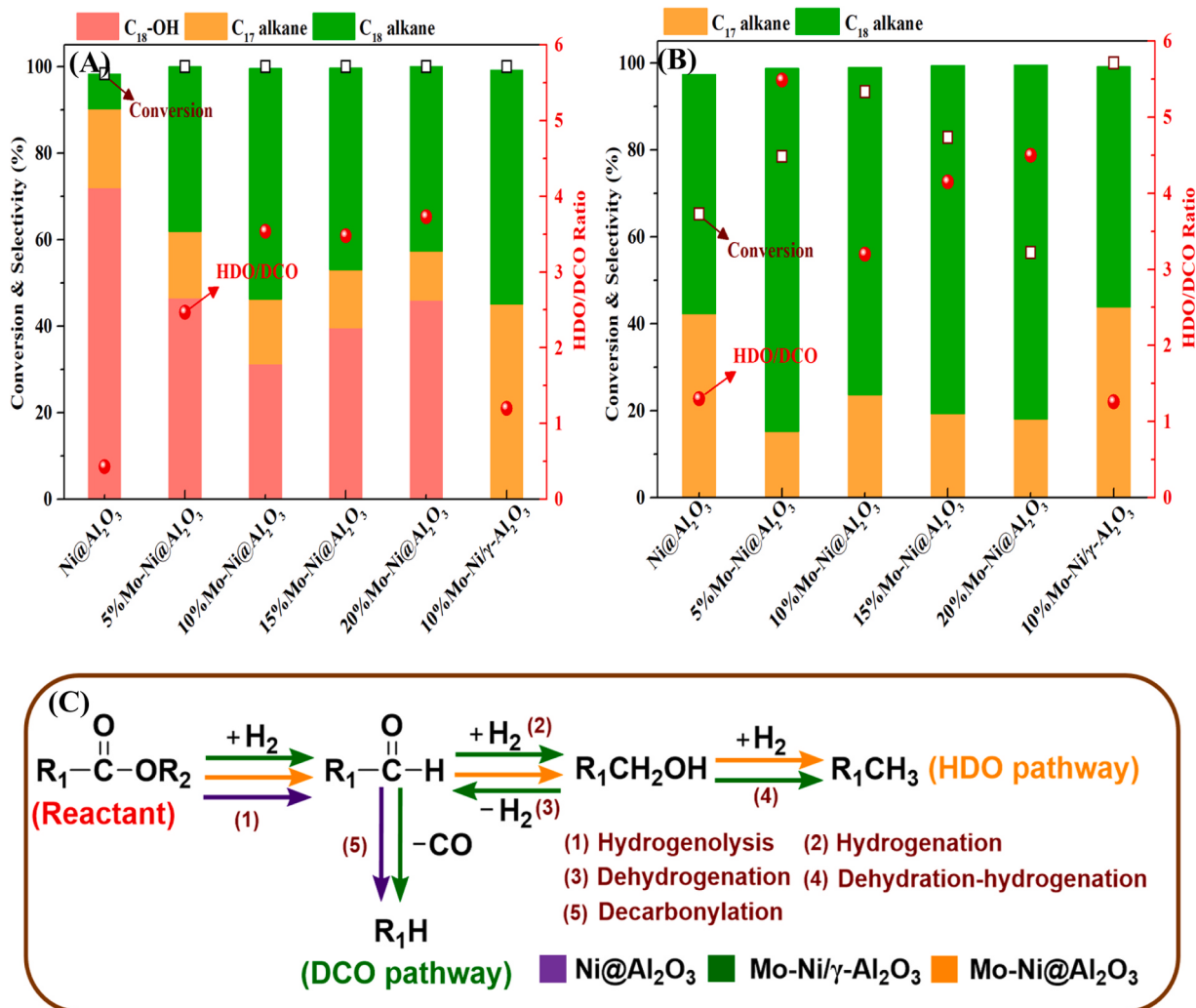


Fig. 7. (A) Conversions of 1-octadecanal (C₁₈-CHO) and (B) of 1-octadecanol (C₁₈-OH) on the different catalysts; (C) Reaction pathway of fatty acid esters over the Ni@Al₂O₃, Mo-Ni/γ-Al₂O₃ and Mo-Ni@Al₂O₃ catalysts. Reaction conditions: reactant (0.1 g), catalyst (0.03 g), n-hexane (10 mL), 230 °C, 3.0 MPa H₂, 45 min.

induced by unsaturated metal sites (Mo^{5+}) facilitates the activation of fatty acid esters and the dehydration-hydrogenation process of fatty alcohol intermediates [46], which results in a high HDO performance.

As for the difference between 10% Mo-Ni/ γ -Al₂O₃ and 10% Mo-Ni@Al₂O₃ catalysts, according to the above catalyst characterization (Figs. 1–4), it is known that it mainly reflects in the particle size of the metallic nickel and the dispersion of metal species on the catalyst surface. Compared with the 10% Mo-Ni/ γ -Al₂O₃ catalyst with large and isolated metallic nickel nanoparticles, the Ni metal nanoparticles are not only highly dispersed on the surface of 10% Mo-Ni@Al₂O₃ catalyst but also closely surrounded by Mo species (as displayed in the Fig. 1(D)). The closely contacted Ni and Mo species are helpful to facilitate the dehydration-hydrogenation process of intermediate C₁₈-OH via enhancing the synergy between them while to suppress the dehydrogenation-decarbonylation process caused by the isolated-monometallic Ni nanoparticles, which improves the selectivity of C_n alkanes without carbon atoms loss.

To further obtain the adsorbed information of fatty aldehyde intermediate on the 10% Mo-Ni@Al₂O₃ and 10% Mo-Ni/ γ -Al₂O₃ catalysts, in-situ FTIR of octanal was performed and the results are shown in Fig. 8. Both spectra showed two bands centred at about 2713 and 1737 cm⁻¹, which correspond to the aldehydic C-H bond and the C=O group of octanal, respectively. Compared with the spectra of Mo-Ni/ γ -Al₂O₃ catalyst (Fig. 8(B)), the band of aldehydic C-H (2713 cm⁻¹) disappeared in the spectra of Mo-Ni@Al₂O₃ (Fig. 8(A)) when the temperature increased to 130 °C. Moreover, it was found that the band at 1737 cm⁻¹ corresponding to the C=O group shifted to a lower wavenumber (1712 cm⁻¹) with the temperature increased from 50 to 150 °C. These

results indicate that there is a stronger interaction between the aldehyde group of octanal and the Mo-Ni@Al₂O₃ catalyst as compared with the Mo-Ni/ γ -Al₂O₃ catalyst. This strong interaction can promote the conversion of fatty aldehydes into the corresponding alcohols via activating its carbonyl group (Fig. 8(C)), and then producing the alkanes without any carbon atoms loss via the dehydration-hydrogenation process, as shown in Fig. S5. In contrast, due to the uneven-distribution of the metal species on the Mo-Ni/ γ -Al₂O₃ catalyst and the appearance of the large and isolated metallic Ni nanoparticles (Fig. 2(A)), the decarbonylation reaction is more likely to occur on the surface of Mo-Ni/ γ -Al₂O₃ catalyst via adsorbing the C-C bond on the two adjacent Ni atoms (Fig. 8(D)) [43], which results in the cleavage of C-C bonds and a low HDO/DCO ratio. Based on the above control experiments and characterizations, it is concluded that the excellent HDO performance of the Mo-Ni@Al₂O₃ is mainly attributed to the well-distribution of Ni and Mo species, which not only suppresses the C-C bonds cleavage caused by isolated monometallic Ni nanoparticles, but also enhances the synergistic promoting effect between them in the conversion of fatty acid esters.

4. Conclusions

In this work, a novel Mo-Ni@Al₂O₃ catalyst was synthesized by virtue of the hydrolysis of AlN support, and then used for selectively hydrogenating fatty acid esters into diesel-range alkanes. Compared with the conventional Mo-Ni/ γ -Al₂O₃ catalyst with the DCO as the main reaction pathway, HDO reaction was dominant on the Mo-Ni@Al₂O₃ catalyst, thereby improving the carbon atom utilization of fatty acid esters. Detailed characterization and control experiments suggest that

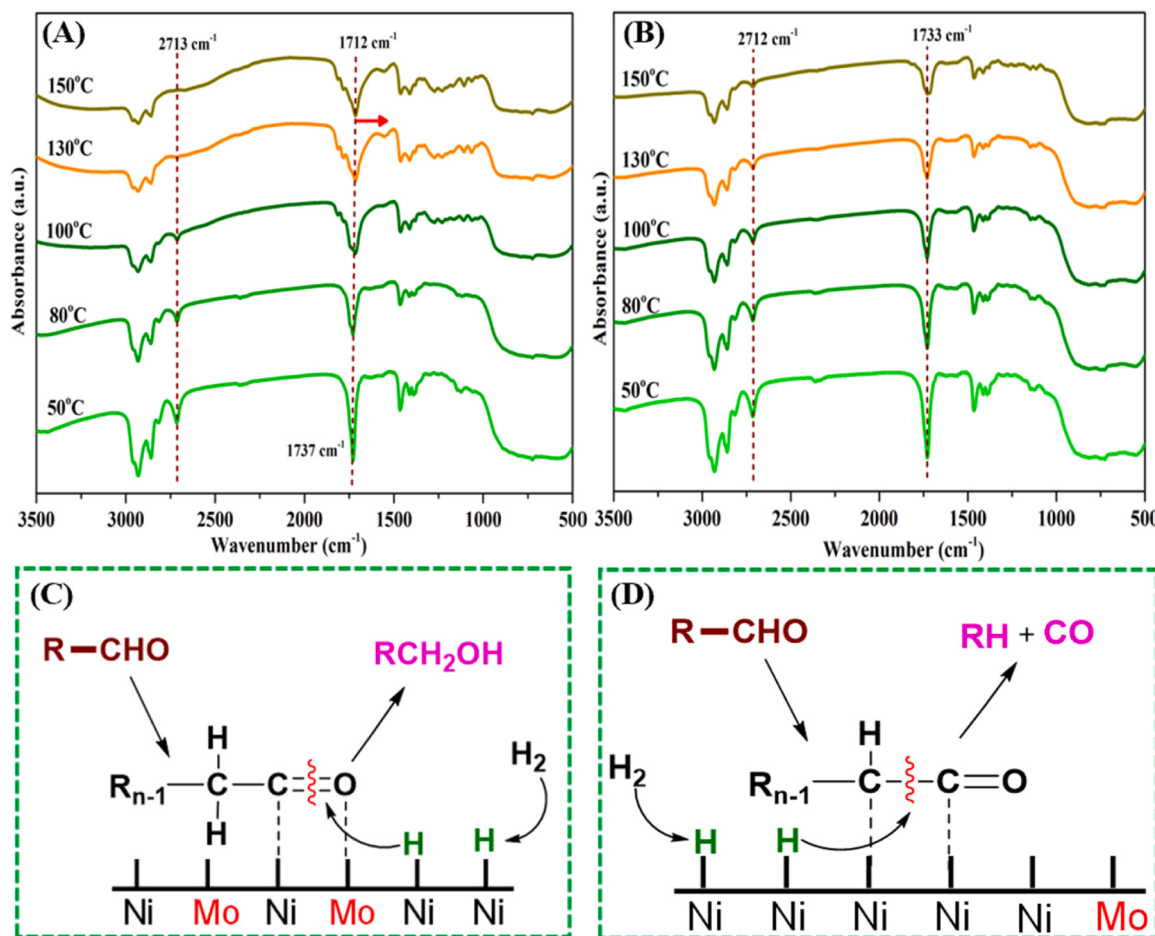


Fig. 8. In-situ IR spectra of octanal adsorption on the (A) 10% Mo-Ni@Al₂O₃ and (B) 10% Mo-Ni/ γ -Al₂O₃ catalysts under hydrogen flow; Adsorption model of fatty aldehydes on the (C) Mo-Ni@Al₂O₃ and (D) Mo-Ni/ γ -Al₂O₃ catalysts.

the improved HDO selectivity of the Mo-Ni@Al₂O₃ catalyst can be attributed to the well-distribution of Ni and Mo species, that is, the intimately contacted Ni and Mo active sites enhances the synergy between these two sites and inhibits the cleavage of C—C bonds induced by isolated single-metal Ni site. In addition, the large specific surface area and pore size also play an important role in enhancing the HDO performance of the Mo-Ni@Al₂O₃ by promoting the reactant molecular diffusion and enhancing the accessibility of active sites. This work provides a green and facile method to synthesize Al₂O₃-supported Ni-Mo bimetallic catalysts with large surface area, high metal dispersion and adjacent Ni and Mo sites, and may also open up a new way for the synthesis of advanced aluminum-supported metal catalysts for heterogeneous catalysis.

CRediT authorship contribution statement

Xincheng Cao: Validation, Formal analysis, Investigation, Writing – original draft. **Shiyu Wu:** Investigation, Formal analysis. **Jiaping Zhao:** Methodology, Formal analysis. **Feng Long:** Conceptualization, Methodology. **Shuya Jia:** Validation. **Xiaolei Zhang:** Validation, Writing-review, Formal analysis. **Junming Xu:** Conceptualization, Methodology, Formal analysis, Writing – review & editing. **Jianchun Jiang:** Conceptualization, Methodology, Writing – review & editing.

Declaration of Competing Interest

The authors declare that they have no known competing financial interests or personal relationships that could have appeared to influence the work reported in this paper.

Data Availability

Data will be made available on request.

Acknowledgements

The authors would like to thank the financial support provided by the Scientific Research Funds of Huaqiao University and the National Natural Science Foundation of China (2019YFB1504005 and 2019YFB1504000).

Appendix A. Supporting information

Supplementary data associated with this article can be found in the online version at [doi:10.1016/j.apcatb.2023.123506](https://doi.org/10.1016/j.apcatb.2023.123506).

References

- [1] A. Bohre, B. Saha, M.M. Abu-Omar, Catalytic upgrading of 5-hydroxymethylfurfural to drop-in biofuels by solid base and bifunctional metal-acid catalysts, *ChemSusChem* 8 (2015) 4022–4029.
- [2] A.D. Sutton, F.D. Waldie, R. Wu, M. Schlaif, L.A. Pete' Silks, J.C. Gordon, The hydrodeoxygenation of bioderived furans into alkanes, *Nat. Chem.* 5 (2013) 428–432.
- [3] M. Hajari, M. Tabatabaei, M. Aghbashlo, H. Ghanavati, A review on the prospects of sustainable biodiesel production: a global scenario with an emphasis on waste-oil biodiesel utilization, *Renew. Sustain. Energy Rev.* 72 (2017) 445–464.
- [4] L. Yan, X.X. Liu, J. Deng, Y. Fu, Molybdenum modified nickel phyllosilicates as a high performance bifunctional catalyst for deoxygenation of methyl palmitate to alkanes under mild conditions, *Green. Chem.* 19 (2017) 4600–4609.
- [5] S.Y. Xing, Y. Liu, X.C. Liu, M. Li, J.Y. Fu, P.F. Liu, P.M. Lv, Z.M. Wang, Solvent-free hydrodeoxygenation of bio-lipids into renewable alkanes over NiW bimetallic catalyst under mild conditions, *Appl. Catal. B: Environ.* 269 (2020) 1–11.
- [6] Y.C. Sharma, B. Singh, J. Korstad, A critical review on recent methods used for economically viable and eco-friendly development of microalgae as a potential feedstock for synthesis of biodiesel, *Green. Chem.* 13 (2011) 2993–3006.
- [7] G.Y. Xu, Y. Zhang, Y. Fu, Q.X. Guo, Efficient hydrogenation of various renewable oils over Ru-HAP catalyst in water, *ACS Catal.* 7 (2017) 1158–1169.
- [8] J.M. Liang, Z.Y. Zhang, K.J. Wu, Y.C. Shi, W.H. Pu, M.D. Yang, Y.L. Wu, Improved conversion of stearic acid to diesel-like hydrocarbons by carbon nanotubes-supported CuCo catalysts, *Fuel Process. Technol.* 188 (2019) 153–163.
- [9] Z.H. Zhang, Q.W. Yang, H. Chen, K.Q. Chen, X.Y. Lu, P.K. Ouyang, J. Fu, J.G. Chen, In situ hydrogenation and decarboxylation of oleic acid into heptadecane over a Cu-Ni alloy catalyst using methanol as a hydrogen carrier, *Green. Chem.* 20 (2018) 197–205.
- [10] H.S. Roh, I.H. Eum, D.W. Jeong, B.E. Yi, J.G. Na, C.H. Ko, The effect of calcination temperature on the performance of Ni/MgO-Al₂O₃ catalysts for decarboxylation of oleic acid, *Catal. Today* 164 (2011) 457–460.
- [11] B.X. Peng, X.G. Yuan, C. Zhao, J.A. Lercher, Stabilizing catalytic pathways via redundancy: selective reduction of microalgae oil to alkanes, *J. Am. Chem. Soc.* 134 (2012) 9400–9405.
- [12] Q.N. Xia, X.J. Zhuang, M.M.J. Li, Y.K. Peng, G.L. Liu, T.S. Wu, Y.L. Soo, X.Q. Gong, Y.Q. Wang, S.C.E. Tsang, Cooperative catalysis for the direct hydrodeoxygenation of vegetable oils into diesel-range alkanes over Pd/Nb₂O₇, *Chem. Commun.* 52 (2016) 5160–5163.
- [13] X.C. Cao, J.P. Zhao, F. Long, X.L. Zhang, J.M. Xu, J.C. Jiang, Al-modified Pd@mSiO₂ core-shell catalysts for the selective hydrodeoxygenation of fatty acid esters: influence of catalyst structure and Al atoms incorporation, *Appl. Catal. B: Environ.* 305 (2022) 1–11.
- [14] Y. Takeda, M. Tamura, Y. Nakagawa, K. Okumura, K. Tomishige, Characterization of Re-Pd/SiO₂ catalysts for hydrogenation of stearic acid, *ACS, Catalysis* 5 (2015) 7034–7047.
- [15] Y. Shao, Q.N. Xia, X.H. Liu, G.Z. Lu, Y.Q. Wang, Pd/Nb₂O₇/SiO₂ catalyst for the direct hydrodeoxygenation of biomass-related compounds to liquid alkanes under mild conditions, *ChemSusChem* 8 (2015) 1761–1767.
- [16] N. Chen, Y. Ren, E.W. Qian, Elucidation of the active phase in PtSn/SAPO-11 for hydrodeoxygenation of methyl palmitate, *J. Catal.* 334 (2016) 79–88.
- [17] Y.T. Zheng, Y. Qi, Z.Y. Tang, F.L. Hanke, S.G. Podkolzin, Kinetics and reaction mechanisms of acetic acid hydrodeoxygenation over Pt and Pt-Mo catalysts, *ACS Sustain. Chem. Eng.* 10 (2022) 5212–5224.
- [18] S.B. Liu, S.K. Dutta, W.Q. Zheng, N.S. Gould, Z.W. Cheng, B.J. Xu, B. Saha, D. Vlachos, Catalytic hydrodeoxygenation of high carbon furylmethanes to renewable jet-fuel ranged alkanes over a rhenium-modified iridium catalyst, *ChemSusChem* 10 (2017) 3225–3234.
- [19] S.B. Liu, W.Q. Zheng, J.Y. Fu, K. Alexopoulos, B. Saha, D.G. Vlachos, Molybdenum oxide-modified iridium catalysts for selective production of renewable oils for jet and diesel fuels and lubricants, *ACS Catal.* 9 (2019) 7679–7689.
- [20] L. Di, S.K. Yao, S. Song, G.J. Wu, W.L. Dai, N.J. Guan, L.D. Li, Robust ruthenium catalysts for the selective conversion of stearic acid to diesel-range alkanes, *Appl. Catal. B: Environ.* 201 (2017) 137–149.
- [21] J.Z. Chen, Q.Y. Xu Hydrodeoxygenation of biodiesel-related fatty acid methyl esters to diesel-range alkanes over zeolite-supported ruthenium catalysts, *Catal. Sci. Technol.* 6 (2016) 7239–7251.
- [22] A. Srifa, K. Faungnawakij, V. Itthibenchapong, S. Assabumrungrat, Roles of monometallic catalysts in hydrodeoxygenation of palm oil to green diesel, *Chem. Eng. J.* 278 (2015) 249–258.
- [23] G.J. Wu, N. Zhang, W.L. Dai, N.J. Guan, L.D. Li, Construction of bifunctional Co/H-ZSM-5 catalysts for the hydrodeoxygenation of stearic acid to diesel-range alkanes, *ChemSusChem* 11 (2018) 2179–2188.
- [24] Y.D. Zhou, X.D. Liu, P. Yu, C.W. Hu, Temperature-tuned selectivity to alkanes or alcohol from ethyl palmitate deoxygenation over zirconia-supported cobalt catalyst, *Fuel* 278 (2020) 1–13.
- [25] X.C. Cao, F. Long, Q.L. Zhai, P. Liu, J.M. Xu, J.C. Jiang, Enhancement of fatty acids hydrodeoxygenation selectivity to diesel-range alkanes over the supported Ni-MoO_x catalyst and elucidation of the active phase, *Renew. Energy* 162 (2020) 2113–2125.
- [26] J.L. Chen, D.C. Wang, F.Q. Luo, X.Y. Yang, X.Y. Li, S.R. Li, Y.Y. Ye, D. Wang, Z. F. Zheng, Selective production of alkanes and fatty alcohol via hydrodeoxygenation of palmitic acid over red mud-supported nickel catalysts, *Fuel* 314 (2022) 1–10.
- [27] Z.Y. Pan, R.J. Wang, J.X. Chen, Deoxygenation of methyl laurate as a model compound on Ni-Zn alloy and intermetallic compound catalysts: geometric and electronic effects of oxophilic Zn, *Appl. Catal. B: Environ.* 224 (2018) 88–100.
- [28] J. Ni, W.H. Leng, J. Mao, J.G. Wang, J.Y. Lin, D.H. Jiang, X.N. Li Tuning, electron density of metal nickel by support defects in Ni/ZrO₂ for selective hydrogenation of fatty acids to alkanes and alcohols, *Appl. Catal. B: Environ.* 253 (2019) 170–178.
- [29] E. Kordouli, B. Pawelec, K. Bourikas, C. Kordulis, J.L.G. Fierro, A. Lycurghiotis, Mo promoted Ni-Al₂O₃ co-precipitated catalysts for green diesel production, *Appl. Catal. B: Environ.* 229 (2018) 139–154.
- [30] E. Kordouli, B. Pawelec, C. Kordulis, A. Lycurghiotis, J.L.G. Fierro, Hydrodeoxygenation of phenol on bifunctional Ni-based catalysts: effects of Mo promotion and support, *Appl. Catal. B: Environ.* 238 (2018) 147–160.
- [31] P. Vozka, D. Orazgaliyeva, P. Simánek, J. Blažek, G. Kilaz, Activity comparison of Ni-Mo/Al₂O₃ and Ni-Mo/TiO₂ catalysts in hydropyrolysis of middle petroleum distillates and their blend with rapeseed oil, *Fuel Process. Technol.* 167 (2017) 684–694.
- [32] J. Li, M. Nakamura, T. Shirai, K. Matsumaru, C. Ishizaki, K. Ishizaki, Mechanism and kinetics of aluminum nitride powder degradation in moist air, *J. Am. Ceram. Soc.* 89 (2006) 937–943.
- [33] S.Q. Li, Y. Fu, W.B. Kong, B.G. Pan, C.K. Yuan, F.F. Cai, H. Zhu, J. Zhang, Y.H. Sun, Dually confined Ni nanoparticles by room-temperature degradation of AlN for dry reforming of methane, *Appl. Catal. B: Environ.* 277 (2020) 1–10.
- [34] X.C. Cao, F. Long, F. Wang, J.P. Zhao, J.M. Xu, J.C. Jiang, Chemoselective decarboxylation of higher aliphatic esters to diesel-range alkanes over the NiCu/Al₂O₃ bifunctional catalyst under mild reaction conditions, *Renew. Energy* 180 (2021) 1–13.

[35] K.S. Sing, Reporting physisorption data for gas/solid systems with special reference to the determination of surface area and porosity, *Pure Appl. Chem.* 57 (1985) 603–619.

[36] J.Q. Jiao, J.Y. Fu, Y.C. Wei, Z. Zhao, A.J. Duan, C.M. Xu, J.M. Li, H. Song, P. Zheng, X.L. Wang, Y.N. Yang, Y. Liu, Al-modified dendritic mesoporous silica nanospheres-supported NiMo catalysts for the hydrodesulfurization of dibenzothiophene: efficient accessibility of active sites and suitable metal–support interaction, *J. Catal.* 356 (2017) 269–282.

[37] A. Srifa, R. Kaewmeesri, C. Fang, V. Itthibenchapong, K. Faungnawakij, NiAl₂O₄ spinel-type catalysts for deoxygenation of palm oil to green diesel, *Chem. Eng. J.* 345 (2018) 107–113.

[38] M.S. Yancheshmeh, O.A. Sahraei, M. Aissaoui, M.C. Iliuta, A novel synthesis of NiAl₂O₄ spinel from a Ni-Al mixed-metal alkoxide as a highly efficient catalyst for hydrogen production by glycerol steam reforming, *Appl. Catal. B: Environ.* 265 (2020) 1–18.

[39] N. Pegios, V. Bliznuk, S.A. Theofanidis, V.V. Galvita, G.B. Marin, R. Palkovits, K. Simeonov, Ni nanoparticles and the kirkendall effect in dry reforming of methane, *Appl. Surf. Sci.* 452 (2018) 239–247.

[40] K. Chandra Mouli, S. Mohanty, Y. Hu, A. Dalai, J. Adjaye, Effect of heteroatom on dispersion of NiMo phase on M-SBA-15 (M=Zr, Ti, Ti-Zr), *Catal. Today* 207 (2013) 133–144.

[41] F.F. Yang, N.J. Libretto, M.R. Komarneni, W. Zhou, J.T. Miller, X. Zhu, D. E. Resasco, Enhancement of m-cresol hydrodeoxygenation selectivity on Ni catalysts by surface decoration of MoO_x species, *ACS, Catalysis* 9 (2019) 7791–7800.

[42] I.E. Wachs, Raman and IR studies of surface metal oxide species on oxide supports: supported metal oxide catalysts, *Catal. Today* 27 (1996) 437–455.

[43] N. Chen, S.F. Gong, E.W. Qian, Effect of reduction temperature of NiMoO_{3-x}/SAPO-11 on its catalytic activity in hydrodeoxygenation of methyl laurate, *Appl. Catal. B: Environ.* 174 (2015) 253–263.

[44] D. Zhang, W.Q. Liu, Y.A. Liu, U. Etim, X.M. Liu, Z.F. Yan, Pore confinement effect of MoO₃/Al₂O₃ catalyst for deep hydrodesulfurization, *Chem. Eng. J.* 330 (2017) 706–717.

[45] J.L. Li, M. Zhang, Z.J. Guan, Q.Y. Li, C.Q. He, J.J. Yang, Synergistic effect of surface and bulk single-electron-trapped oxygen vacancy of TiO₂ in the photocatalytic reduction of CO₂, *Appl. Catal. B: Environ.* 206 (2017) 300–307.

[46] S. Janampelli, S. Darbha, Selective deoxygenation of fatty acids to fuel-range hydrocarbons over Pt-MO_x/ZrO₂ (M = Mo and W) catalysts, *Catal. Today* 375 (2021) 174–180.